Eur. Phys. J. A **24**, 459–474 (2005)
DOI 10.1140/epja/i2004-10234-2

THE EUROPEAN PHYSICAL JOURNAL A

Charged lepton production from iron induced by atmospheric neutrinos

M. Sajjad Athar, S. Ahmad, and S.K. Singh[a]

Department of Physics, Aligarh Muslim University, Aligarh - 202 002, India

Received: 30 September 2004 / Revised version: 12 April 2005 /
Published online: 8 June 2005 –
Communicated by G. Orlandini

Abstract. The charged current lepton production induced by neutrinos in ^{56}Fe nuclei has been studied. The calculations have been done for the quasielastic as well as the inelastic reactions assuming Δ-dominance and take into account the effect of Pauli blocking, Fermi motion and the renormalization of weak transition strengths in the nuclear medium. The quasielastic production cross-sections for lepton production are found to be strongly reduced due to nuclear effects, while there is about 10% reduction in the inelastic cross-sections in the absence of the final-state interactions of the pions. The numerical results for the momentum and angular distributions of the leptons averaged over the various atmospheric-neutrino spectra at the Soudan and Gran Sasso sites have been presented. The effect of nuclear-model dependence and the atmospheric-flux dependence on the relative yield of μ to e has been studied and discussed.

PACS. 25.30.Pt Neutrino scattering – 13.15.+g Neutrino interactions – 23.40.Bw Weak-interaction and lepton (including neutrino) aspects – 21.60.Jz Hartree-Fock and random-phase approximations

1 Introduction

The study of neutrino physics with atmospheric neutrinos has a long history with first observations of muons produced by atmospheric muon neutrinos in deep underground laboratories of KGF in India and ERPM in South Africa [1]. The indications of some deficit in the atmospheric-neutrino flux was known to exist from the early days of these experiments but the evidence was no more than suggestive due to low statistics of the experimental data and anticipated uncertainties in the flux calculations [2]. The clear evidence of a deficit in the atmospheric muon neutrino flux was confirmed later when data with better statistics were obtained at IMB [3], Kamiokande [4] and Soudan [5] experiments. The most likely cause of this deficit is believed to be the phenomena of neutrino oscillations [6] in which the neutrinos produced with muon flavor after passing a certain distance through the atmosphere, manifest themselves as a different flavor. The implication of this phenomena of neutrino oscillation is that neutrinos possess a nonzero mass pointing towards physics beyond the standard model of particle physics. The evidence for neutrino oscillations and a nonzero mass for the neutrinos has also been obtained in the observations made with solar [7] and reactor (anti)neutrinos [8].

It is well known that, in a two-flavor oscillation scenario involving muon neutrino, the probability for a muon neutrino with energy E_ν to remain a muon neutrino after propagating a distance L before reaching the detector is given by [6]

$$P_{\mu\mu} = 1 - \sin^2 2\theta \sin^2 \left(\frac{1.27 \Delta m^2\,(\mathrm{eV}^2) L\,(\mathrm{km})}{E_\nu\,(\mathrm{GeV})} \right) \quad (1)$$

where $\Delta m^2 = m_1^2 - m_2^2$ is the difference of the squared masses of the two flavor mass eigenstates and θ is the mixing angle between two states. The oscillation parameters Δm^2 and the mixing angle θ are determined by various observations made in atmospheric-neutrino experiments. These include the flavor ratios of muon and electron flavors, angular and $\frac{L}{E}$ distributions of muons and electrons produced by atmospheric neutrinos. The first claims of seeing neutrino oscillation in atmospheric neutrinos came from the measurements of ratio of ratios R_ν defined as $\frac{(\mu/e)_{\mathrm{data}}}{(\mu/e)_{\mathrm{MC}}}$ from the observations of fully contained (FC) events [3,4], but there are now data available from the angular and $\frac{L}{E}$ distribution of the atmospheric-neutrino–induced muon and electron events from SK [9], MACRO [10] and Soudan [11] experiments which confirm the phenomena of neutrino oscillations. These experiments are consistent with a value of $\Delta m^2 \approx 3.2 \times 10^{-3}\,\mathrm{eV}^2$ and $\sin^2 2\theta \approx 1$. The analysis of these data assuming a three-flavor neutrino oscillation phenomenology has also been done by many authors [12].

[a] e-mail: pht13sks@rediffmail.com

The major sources of uncertainty in the theoretical prediction of the charged leptons of muon and electron flavor produced by the atmospheric neutrinos come from the uncertainties in the calculation of atmospheric-neutrino fluxes and neutrino nuclear cross-sections. The atmospheric-neutrino fluxes at various experimental sites of Kamioka, Soudan and Gran Sasso have been extensively discussed in the literature by many authors [13–16]. The neutrino nuclear cross-sections have also been calculated for various nuclei by many authors using different nuclear models [17–24]. The aim of the present paper is to study the neutrino nuclear cross-section in iron nuclei which are relevant for the atmospheric-neutrino experiments performed at Soudan [11], FREJUS [25] and NUSEX [26] and planned in the future with MINOS [27], MONOLITH [28] and INO [29] detectors. The uncertainty in the nuclear production cross-section of leptons from iron nuclei by the atmospheric neutrinos are discussed. For our nuclear model, we also discuss the uncertainty due to the use of different neutrino fluxes for the sites of Soudan and Gran Sasso which are relevant to MINOS, MONOLITH and INO detectors [27–29].

The momentum and angular distribution of muons and electrons relevant to fully contained events produced by atmospheric neutrinos in iron nuclei are calculated. These leptons of muon and electron flavor characterized by track and shower events include the leptons produced by quasielastic process as well as the inelastic processes induced by charged current interactions. The calculations are done in a model which takes into account nuclear effects like Pauli Blocking, Fermi motion effects and the effect of renormalization of the weak transition strengths in nuclear medium in local density approximation. The model has been successfully applied to describe various electromagnetic and weak processes like photon absorption, electron scattering, muon capture and low-energy neutrino reactions in nuclei [24,30–32]. The model can be easily applied to calculate the zenith angle dependence and the $\frac{L}{E}$ distribution for stopping and thorough going muon production from iron nuclei which is currently under progress.

The plan of the paper is as follows. In sect. 2 we describe the neutrino (antineutrino) quasielastic inclusive production of leptons (e^-, μ^-, e^+, μ^+) from iron nuclei for various neutrino energies. In sect. 3 we describe the energy dependence of the inelastic production of leptons through the Δ-dominance model and highlight the nuclear effects relevant to the energy of fully contained events. In sect. 4, we use the atmospheric-neutrino flux at Soudan and Gran Sasso sites as determined by various authors and discuss the flux-averaged momentum and angular dependence of leptons corresponding to different flux calculations available at these two sites.

2 Quasielastic production of leptons

Quasielastic inclusive production of leptons in nuclei induced by neutrinos has been studied by many authors [17–24], where nuclear effects have been calculated. Most of these calculations have been done either for ^{16}O relevant to IMB and Kamioka experiments [3,4] or for ^{12}C relevant to LSND and KARMEN experiments [33]. These calculations generally use a direct summation method (over many nuclear excited states) [17], closure approximation [18], Fermi gas model [19,20], relativistic mean-field approximation [21], continuum random phase approximation (CRPA) [22] and local density approximation [23,24]. The calculations for ^{56}Fe nucleus have been reported by Bugaev *et al.* [17] in a shell model and in Fermi gas model by Gallagher [34] and Berger *et al.* [35]. In this section we briefly describe the formalism and results of our calculations done for quasielastic inclusive production of leptons for iron nuclei.

2.1 Formalism

In local density approximation the neutrino nucleus cross-section $\sigma(E_\nu)$ for a neutrino of energy E_ν scattering from a nucleus $A(Z,N)$, is given by

$$\sigma^A(E_\nu) = 2\int \mathrm{d}\vec{r}\frac{\mathrm{d}\vec{p}}{(2\pi)^3} n_n(\vec{p},\vec{r})\sigma^N(E_\nu)\,, \qquad (2)$$

where $n_n(\vec{p},\vec{r})$ is the local occupation number of the initial nucleon of momentum $\vec{p}$ (localized at position $\vec{r}$ in the nucleus) and $\sigma^N(E_\nu)$ is the cross-section for the scattering of neutrino of energy E_ν from a free nucleon given by the expression

$$\sigma^N(E_\nu) = \int \frac{\mathrm{d}^3k'}{(2\pi)^3}\frac{m_\nu}{E_\nu}\frac{m_e}{E_e}\frac{M_n}{E_n}\frac{M_p}{E_p} \times\overline{\sum}\sum |T|^2\delta(E_\nu - E_l + E_n - E_p)\,, \qquad (3)$$

where T is the matrix element for the basic process

$$\nu_l(k) + n(p) \to l^-(k') + p(p'), \quad l = e,\mu \qquad (4)$$

written as

$$T = \frac{G_\mathrm{F}}{\sqrt{2}}\cos\theta_\mathrm{c}\ \bar{u}(k')\gamma_\mu(1-\gamma_5)u(k)\ (J^\mu)^\mathrm{CC}\,; \qquad (5)$$

$(J^\mu)^\mathrm{CC}$ is the charged current (CC) matrix element of the hadronic current defined as

$$(J^\mu)^\mathrm{CC} = \bar{u}(p')\left[F_1^V(q^2)\gamma^\mu + F_2^V(q^2)i\sigma^{\mu\nu}\frac{q_\nu}{2M} + F_A^V(q^2)\gamma^\mu\gamma^5\right]u(p)\,; \qquad (6)$$

$q^2(q = k-k')$ is the four-momentum transfer squared. The form factors $F_1^V(q^2)$, $F_2^V(q^2)$ and $F_A^V(q^2)$ are isovector electroweak form factors written as

$$F_1^V(q^2) = F_1^p(q^2) - F_1^n(q^2),$$
$$F_2^V(q^2) = F_2^p(q^2) - F_2^n(q^2),$$
$$F_A^V(q^2) = F_A(q^2),$$

where

$$F_1^{p,n}(q^2) = \frac{1}{\left(1-\frac{q^2}{4M^2}\right)}\left[G_E^{p,n}(q^2) - \frac{q^2}{4M^2}G_M^{p,n}(q^2)\right],$$

$$F_2^{p,n}(q^2) = \frac{1}{\left(1-\frac{q^2}{4M^2}\right)}\left[G_M^{p,n}(q^2) - G_E^{p,n}(q^2)\right],$$

$$G_E^p(q^2) = \left(1-\frac{q^2}{M_v^2}\right)^{-2}, \qquad (7)$$

$$G_M^p(q^2) = (1+\mu_p)G_E^p(q^2), \qquad G_M^n(q^2) = \mu_n G_E^p(q^2);$$
$$G_E^n(q^2) = \left(\frac{q^2}{4M^2}\right)\mu_n G_E^p(q^2)\xi_n;$$
$$\xi_n = \frac{1}{1-\lambda_n\frac{q^2}{4M^2}}, \qquad \mu_p = 1.79,\ \mu_n = -1.91,$$
$$M_v = 0.84\,\mathrm{GeV}, \qquad \text{and} \quad \lambda_n = 5.6.$$

The isovector axial vector form factor $F_A(Q^2)$ is given by

$$F_A(Q^2) = \frac{F_A(0)}{\left(1-\frac{q^2}{M_A^2}\right)^2}$$

where $M_A = 1.032\,\mathrm{GeV}$; $F_A(0) = -1.261$.

In a nuclear process the neutrons and protons are not free and their momenta are constrained by the Pauli principle which is implemented in this model by requiring that for neutrino reactions initial-nucleon momentum $p \le p_{\mathrm{F}_n}$ and final-nucleon momentum $p' = (|\vec{p}+\vec{q}|) > p_{\mathrm{F}_p}$, where $p_{\mathrm{F}_{n,p}} = [\frac{3}{2}\pi^2\rho_{n,p}(r)]^{\frac{1}{3}}$, are the local Fermi momenta of neutrons and protons at the interaction point in the nucleus defined in terms of their respective nuclear densities $\rho_{n,p}(r)$. These constraints are incorporated while performing the integration over the initial-nucleon momentum in eq. (2) by replacing the energy conserving δ-function in eq. (3) by $-\frac{1}{\pi}\mathrm{Im}U_N(q_0,\vec{q})$, where $U_N(q_0,\vec{q})$ is the Lindhard function corresponding to the particle-hole (ph) excitations induced by the weak interaction process through W exchange shown in fig. 1(a). In the large mass limit of the W-boson, *i.e.* $M_W \to \infty$, fig. 1(a) is reduced to fig. 1(b) for which the imaginary part of the Lindhard function, *i.e.* $\mathrm{Im}U_N(q_0,\vec{q})$, is given by

$$\mathrm{Im}U_N(q_0,\vec{q}) = -\frac{1}{2\pi}\frac{M_p M_n}{|\vec{q}|}\left[E_{\mathrm{F}_1} - A\right] \text{ with} \qquad (8)$$

$$q^2 < 0,\ E_{\mathrm{F}_2} - q_0 < E_{\mathrm{F}_1} \text{ and } \frac{-q_0 + |\vec{q}|\sqrt{1-\frac{4M^2}{q^2}}}{2} < E_{\mathrm{F}_1},$$

where E_{F_1} and E_{F_2} are the local Fermi energy of initial and final nucleons and

$$A = \mathrm{Max}\left[M_n,\ E_{\mathrm{F}_2} - q_0,\ \frac{-q_0 + |\vec{q}|\sqrt{1-\frac{4M^2}{q^2}}}{2}\right].$$

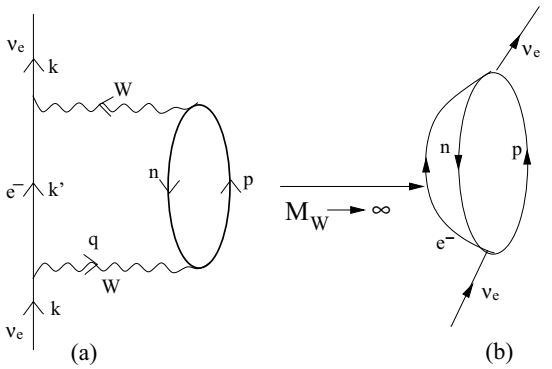

Fig. 1. Diagrammatic representation of the neutrino self-energy diagram corresponding to the ph excitation leading to the $\nu_e + n \to e^- + p$ process in nuclei. In the large mass limit of the W-boson (*i.e.* $M_W \to \infty$) diagram (a) is reduced to (b) which is used to calculate $|T|^2$ in eq. (5).

The expression for the neutrino nuclear cross-section $\sigma^A(E_\nu)$, is then given by

$$\sigma^A(E_\nu) = -\frac{4}{\pi}\int_{r_{\min}}^{r_{\max}} r^2\mathrm{d}r \int_{{p_l}^{\min}}^{{p_l}^{\max}} {p_l}^2\mathrm{d}p_l \int_{-1}^{1}\mathrm{d}(\cos\theta) \times\frac{1}{E_\nu E_l}\overline{\sum}\sum|T|^2\mathrm{Im}U_N[E_\nu - E_l,\ \vec{q}]. \qquad (9)$$

Moreover, in the nucleus, the Q value of the nuclear reaction and the Coulomb distortion of the final lepton in the electromagnetic field of the final nucleus should be taken into account. This is done by modifying the energy conserving δ-function $\delta(E_\nu - E_l + E_n - E_p)$ in eq. (3) to $\delta(E_\nu - Q - (E_l + V_{\mathrm{c}}(r)) + E_n - E_p)$, where $V_{\mathrm{c}}(r)$ is the Coulomb energy of the produced lepton in the field of final nucleus and is given by

$$V_{\mathrm{c}}(r) = ZZ'\alpha 4\pi\left(\frac{1}{r}\int_0^r \frac{\rho_p(r')}{Z}r'^2\mathrm{d}r' + \int_r^\infty \frac{\rho_p(r')}{Z}r'\mathrm{d}r'\right). \qquad (10)$$

This amounts to the evaluation of the Lindhard function in eq. (8) at $(q_0 - (Q + V_{\mathrm{c}}(r)),\ \vec{q})$ instead of $(q_0,\ \vec{q})$. The implementation of this modification requires a judicious choice of the Q value for inclusive nuclear reactions in which many nuclear states are excited in iron. We have taken a Q value of 6.8 MeV corresponding to the transition to the lowest-lying 1^+ state in ^{56}Co for the $\nu_l + {}^{56}\mathrm{Fe} \to l^- + {}^{56}\mathrm{Co}^\star$ reaction and a Q value of 4.3 MeV corresponding to the transition to the lowest-lying 1^+ state in ^{56}Mn for the $\bar{\nu}_l + {}^{56}\mathrm{Fe} \to l^+ + {}^{56}\mathrm{Mn}^\star$ reaction.

The inclusion of $V_{\mathrm{c}}(r)$ to modify energy and corresponding momentum of the charged lepton in the Coulomb field of the final nucleus in our model is equivalent to the treatment of the Coulomb distortion effect in the modified effective momentum approximation (MEMA). This approximation has been used in other calculations of charged current neutrino reactions [36] and electron scattering at higher energies [37].

With these modifications, the final expression for the quasielastic inclusive production from the iron nucleus is

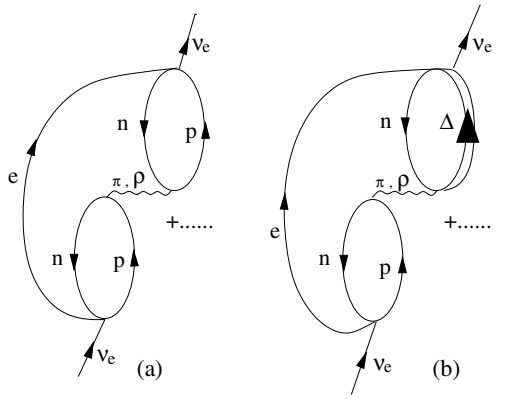

Fig. 2. Many-body Feynman diagrams (drawn in the limit $M_W \to \infty$) accounting for the medium polarization effects contributing to the process $\nu_e + n \to e^- + p$ transitions.

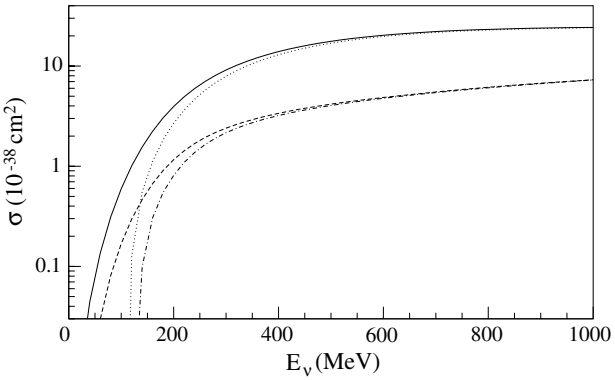

Fig. 3. Total quasielastic cross-sections in the present model for the neutrino and antineutrino reactions in ^{56}Fe are shown by solid line for ν_e, dashed line for $\bar{\nu}_e$, dotted line for ν_μ and dash-dotted line for $\bar{\nu}_\mu$ reactions.

given by

$$\sigma^A(E_\nu) = -\frac{4}{\pi}\int_{r_{\min}}^{r_{\max}} r^2 \mathrm{d}r \int_{{p_l}^{\min}}^{{p_l}^{\max}} {p_l}^2 \mathrm{d}p_l \int_{-1}^{1} \mathrm{d}(\cos\theta) \times \frac{1}{E_\nu E_l}\overline{\sum}\sum |T|^2 \mathrm{Im}U_N[q_0 - (Q + V_c(r)),\ \vec{q}]. \quad (11)$$

It is well known that weak transition strengths are modified in the nuclear medium due to the presence of strongly interacting nucleons. This modification of the weak transitions strength in the nuclear medium is taken into account by considering the propagation of particle-hole (ph) excitations in the medium. While propagating through the medium, the ph excitations interact through the nucleon nucleon potential and create other particle-hole and Δh excitations as shown in fig. 2. The effect of these excitations are calculated in the random phase approximation which is described in refs. [23,32]. The effect of the nuclear medium on the renormalization of weak strengths is treated in a nonrelativistic framework. In the leading order, the nonrelativistic reduction of the weak hadronic current defined in eq. (6), the $F_2(q^2)$ term gives a spin-isospin transition operator $\frac{\vec{\sigma}\times\vec{q}}{2M}\vec{\tau}$ which is a transverse operator, while the $F_A(q^2)$ term gives a spin-isospin transition operator $\vec{\sigma}\cdot\vec{\tau}$ which has a longitudinal as well as a transverse part. This representation of the transition operators in the longitudinal and transverse parts is useful when summing the diagrams in fig. 2 in random phase approximation (RPA) to calculate $|T|^2$. While the charge coupling remains unchanged due to nuclear medium effects, the terms proportional to F_2^2 are affected by the transverse part of the nucleon-nucleon potential, while the terms proportional to F_A^2 are affected by transverse as well as longitudinal parts. The effect is to replace the terms like F_2^2, F_A^2, F_2F_A, etc., in the following manner [23,32]:

$$(F_2^2, F_2F_A) \to (F_2^2, F_2F_A)\frac{1}{|1 - U_N V_t|^2},$$
$$F_A^2 \to \left[\frac{1}{3}\frac{1}{|1 - U_N V_l|^2} + \frac{2}{3}\frac{1}{|1 - U_N V_t|^2}\right], \quad (12)$$

where V_l and V_t are the longitudinal and transverse parts of the nucleon-nucleon potential calculated with π and ρ exchanges and modulated by the Landau-Migdal parameter g' to take into account the short-range correlation effects and are given by

$$V_l(q) = \frac{f^2}{m_\pi^2}\left[\frac{q^2}{-q^2 + m_\pi^2}\left(\frac{\Lambda_\pi^2 - m_\pi^2}{\Lambda_\pi^2 - q^2}\right)^2 + g'\right],$$
$$V_t(q) = \frac{f^2}{m_\pi^2}\left[\frac{q^2}{-q^2 + m_\rho^2}C_\rho\left(\frac{{\Lambda_\rho}^2 - m_\rho^2}{{\Lambda_\rho}^2 - q^2}\right)^2 + g'\right] \quad (13)$$

with $\Lambda_\pi = 1.3\,\mathrm{GeV}$, $C_\rho = 2.0$, $\Lambda_\rho = 2.5\,\mathrm{GeV}$, m_π and m_ρ are the pion and rho-meson masses and g' is taken to be 0.7 [31]. The effect of Δh excitations are taken into account by including the Lindhard function U_Δ for the Δh excitations and replacing U_N by $U_N + U_\Delta$ in eq. (12). The complete expressions for U_N and U_Δ used in our calculations are taken from [38]. The different couplings for N and Δ to the nucleon are incorporated in U_N and U_Δ and then the same interaction strengths V_l and V_t are used for ph and Δh excitations [39,40].

2.2 Results

We present the numerical results for the total cross-section for the quasielastic processes $\nu_l(\bar{\nu}_l) + {}^{56}\mathrm{Fe} \to l^-(l^+) + {}^{56}\mathrm{Co}^\star({}^{56}\mathrm{Mn}^\star)$ as a function of energy for neutrino and antineutrino reactions on iron in the energy region relevant to the fully contained events of atmospheric neutrinos, *i.e.* $E_\nu < 3\,\mathrm{GeV}$. The cross-sections have been calculated using eq. (11) with the nuclear density $\rho(r)$ given by a two-parameter Fermi density [41]: $\rho(r) = \frac{\rho(0)}{1.+\exp(\frac{r-c}{z})}$ with $c = 3.971\,\mathrm{fm}$, $z = 0.5935\,\mathrm{fm}$, $\rho_n(r) = \frac{(A-Z)}{A}\rho(r)$ and $\rho_p(r) = \frac{Z}{A}\rho(r)$.

In fig. 3 we show the numerical results of $\sigma(E)$ *vs.* E, for all flavors of neutrinos, *i.e.* ν_μ, $\bar{\nu}_\mu$, ν_e and $\bar{\nu}_e$. The reduction due to nuclear effects is large at lower energies but

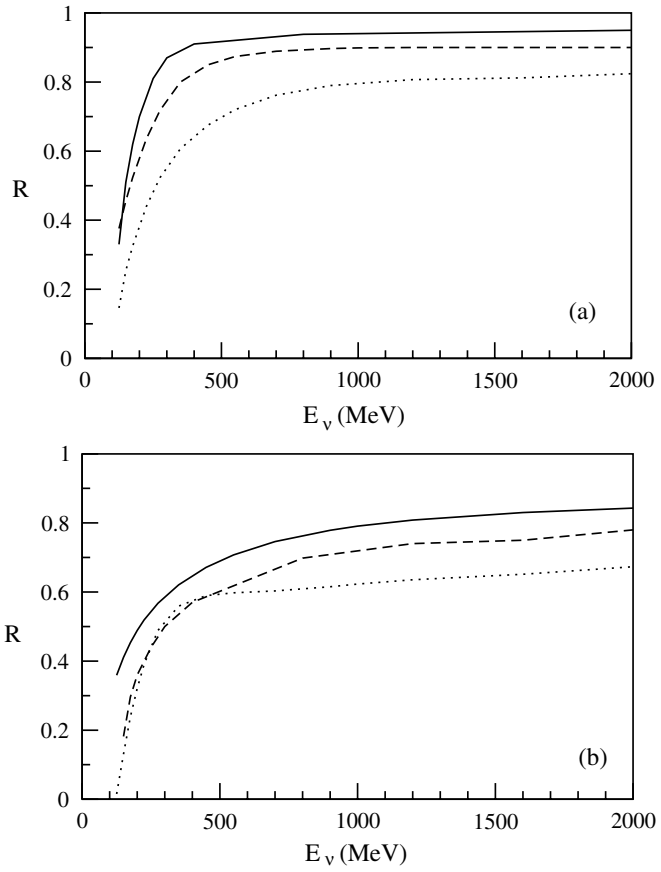

Fig. 4. Ratio of the total cross-section to the free neutrino nucleon cross-section for the reactions (a) $\nu_\mu + n \rightarrow \mu^- + p$ (b) $\bar{\nu}_\mu + p \rightarrow \mu^+ + n$ in iron nuclei in the present model with Pauli suppression (solid line), with nuclear effects (dotted line) and in the Fermi gas model (dashed line) [20].

becomes small at higher energies. The energy dependences of the cross-sections for muon- and electron-type neutrinos are similar except for the threshold effects which are seen only at low energies ($E_\nu < 500$ MeV). This reduction in σ is due to Pauli blocking as well as to the weak renormalization of transition strengths which have been separately shown in fig. 4(a) and (b) for neutrinos and antineutrinos, where we also show the results in the Fermi gas model given by Llewellyn Smith [20]. We plot in fig. 4(a) and (b) for neutrinos and antineutrinos, the reduction factor $R = \frac{\sigma_{\rm nuclear}(E)}{\sigma_{\rm nucleon}(E)}$ *vs.* E, where $\sigma_{\rm nuclear}(E)$ is the cross-section per neutron (proton) for neutrino (antineutrino) reactions in the nuclear medium. The solid lines show the reduction factor R when only the Pauli suppression is taken into account through the imaginary part of the Lindhard function given in eq. (8). This is similar to the results of Llewellyn Smith [20] in the Fermi gas model shown by dashed lines. In this model the total cross-section σ is calculated by using the formula $\sigma = \int {\rm d}q^2 \ R(q^2)(\frac{{\rm d}\sigma}{{\rm d}q^2})_{\rm free}$, where $R(q^2)$ describes the reduction in the cross-section calculated in the Fermi gas model and includes the effect of the Pauli suppression only [20]. However, in our model we get further reduction due to renormalization of weak transition strengths in the nuclear medium when the effects of fig. 2(a) and (b) are included. These are shown by dotted lines in figs. 4(a) and (b). We find that the reduction at higher energies ($E > 1\,{\rm GeV}$) is around 20% for neutrinos and 40% for antineutrinos. It is worth noting that the energy dependence of the reduction due to nuclear medium effects is different for neutrinos and antineutrinos. This is due to the different renormalization of various terms like F_A^2, F_2F_A and F_2^2 in $|T|^2$ which enter in different combinations for neutrino and antineutrino reactions. The results for ν_e and $\bar{\nu}_e$ cross-section are, respectively, similar to ν_μ and $\bar{\nu}_\mu$ reactions except for the threshold effects and are not shown here.

In figs. 5 and 6 we compare our results for $\sigma(E)$ with the results of some earlier experiments which contain nuclear targets like carbon [42], freon [43,44], freon-propane [45] and aluminum [46], where the experimental results for the deuteron targets [47] are not included as they are not subject to the various nuclear effects discussed here. It should be kept in mind that the nuclear targets considered here (except for Br in freon) are lighter than Fe. Therefore, the reduction in the total cross-section due to nuclear effects will be slightly overestimated. For example, for energies $E_\nu \geq 1\,{\rm GeV}$ the reduction in neutrino (antineutrino) cross-section in the case of ^{56}Fe is 5% more than the reduction in the case of ^{12}C [48]. In comparision to the neutrino (antineutrino) nuclear cross-sections as obtained in the Fermi gas model of Llewellyn Smith [20] (shown by dashed lines in figs. 5 and 6) we get a smaller result for these cross-sections. This reduction in the total cross-section leads to an improved agreement with the experimental results as compared to the Fermi gas model results specially for antineutrino reactions (fig. 6). It should be emphasized that the Fermi gas model has no specific mechanism to estimate the renormalization of weak transition strengths in nuclei, while in our model this is incorporated by taking into account the RPA correlations.

In fig. 7(a) and (b), we show the nuclear medium effects on the momentum and angular distributions, *i.e.* $\frac{{\rm d}\sigma}{{\rm d}p_l}$ and $\frac{{\rm d}\sigma}{{\rm d}\cos\theta_l}$ of leptons produced in ν_μ and $\bar{\nu}_\mu$ reactions. We find a large suppression in the results specially in the peak region of momentum and angular distributions. Quantitatively similar results are obtained for the case of ν_e and $\bar{\nu}_e$ reactions and are not shown here.

We have also studied the effect of Coulomb distortion in the momentum distribution of leptons but found no substantial effect around $E_\nu = 1.0\,{\rm GeV}$. These are found to affect the results only at low energies, *i.e.* $E_\nu < 500\,{\rm MeV}$, where the peak is slightly shifted to lower momentum as shown in fig. 8(a) and (b).

3 Inelastic production of leptons

The inelastic production process of leptons is the process in which the production of leptons is accompanied by one-pion (or more pions). There are many calculations of one-pion production by neutrinos from free nucleons [49] but there are only a few calculations which

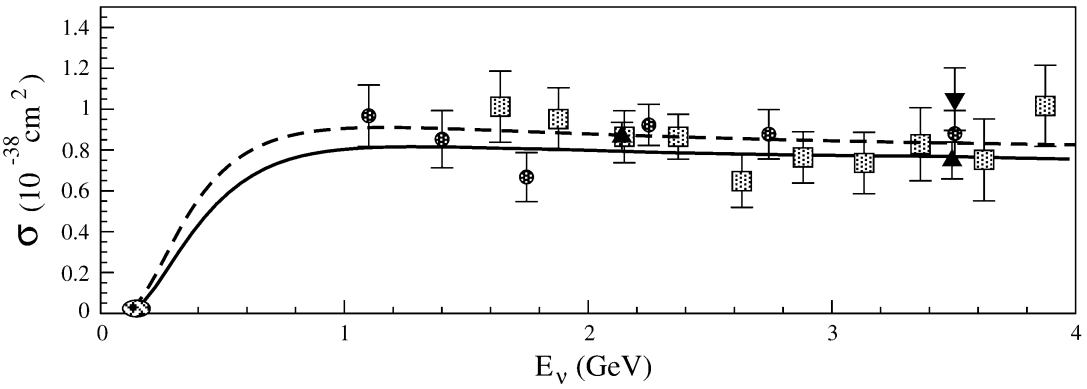

Fig. 5. Neutrino quasielastic total cross-section per nucleon in iron for the $\nu_\mu + n \to p + \mu^-$ reaction. The data are from LSND [42] (ellipse), Bonnetti *et al.* [43] (squares), SKAT Collaboration [44] (triangle down), Pohl *et al.* [45] (circles) and Belikov *et al.* [46] (triangles up). The dashed line is the result of the cross-section in the Fearmi gas model [20] and the solid line is the result using the present model with nuclear effects.

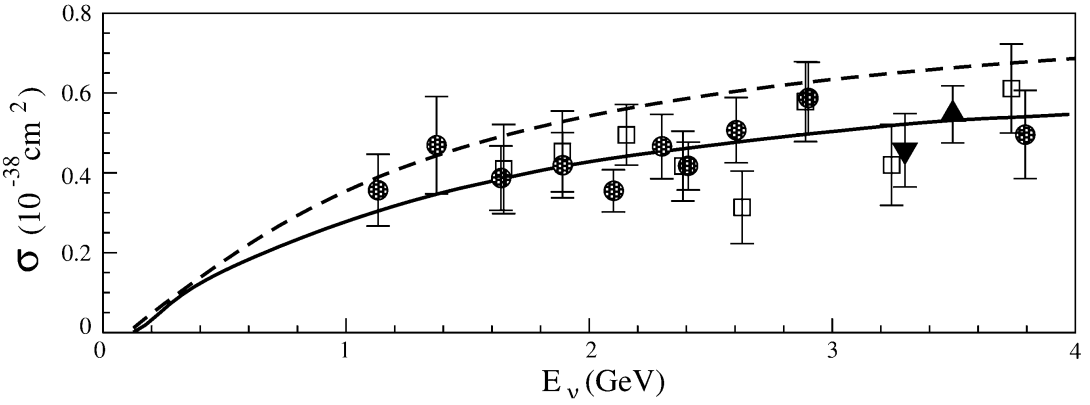

Fig. 6. Antineutrino quasielastic total cross-section per nucleon in iron for the $\bar{\nu_\mu} + p \to n + \mu^+$ reaction. The data are from Bonnetti *et al.* [43], SKAT Collaboration [44] (triangle down), Pohl *et al.* [45] (circles), Belikov *et al.* [46] (triangle up). The dashed line is the result of the cross-section in the Fermi gas model [20] and the solid line is the result using the present model with nuclear effects.

discuss the nuclear effects in these processes [50,52]. In this section we follow the method of ref. [51] to estimate the nuclear effects and nuclear-model dependence of inelastic production cross-section of leptons induced by neutrinos from iron nuclei. The calculations are done assuming Δ-dominance of one-pion production because the contribution of higher resonances in the energy region of atmospheric neutrinos leading to fully contained events is expected to be small.

3.1 Formalism

The matrix element for the neutrino production reaction of Δ on proton targets leading to one-pion events, *i.e.*

$$\nu_l(k) + p(p) \to l^-(k') + \Delta^{++}(p')\,, \tag{14}$$

is given by eq. (5) where J^μ now defines the matrix element of the transition hadronic current between N and Δ states. The most general form of $J^\mu_{\rm CC}$ is written as [51]

$$\begin{aligned} J^\mu_{\rm CC} = \bar{\psi}_\alpha(p')\Bigg[\Bigg(&\frac{C_3^V(q^2)}{M}(g^{\alpha\mu}\not{q} - q^\alpha\gamma^\mu) \\ &+\frac{C_4^V(q^2)}{M^2}(g^{\alpha\mu}q\cdot p' - q^\alpha p'^\mu) \\ &+\frac{C_5^V(q^2)}{M^2}(g^{\alpha\mu}q\cdot p - q^\alpha p^\mu) + \frac{C_6^V(q^2)}{M^2}q^\alpha q^\mu\Bigg)\gamma_5 \\ &+\Bigg(\frac{C_3^A(q^2)}{M}(g^{\alpha\mu}\not{q} - q^\alpha\gamma^\mu) \\ &+\frac{C_4^A(q^2)}{M^2}(g^{\alpha\mu}q\cdot p' - q^\alpha p'^\mu) \\ &+C_5^A(q^2)g^{\alpha\mu} + \frac{C_6^A(q^2)}{M^2}q^\alpha q^\mu\Bigg)\Bigg]u(p)\,, \end{aligned} \tag{15}$$

where $\psi_\alpha(p')$ and $u(p)$ are the Rarita-Schwinger and Dirac spinors for Δ and nucleon of momenta p' and p, respectively, $q(= p' - p = k - k')$ is the momentum transfer and C_i^V $(i = 3\text{–}6)$ are vector and C_i^A $(i = 3\text{–}6)$ are axial vector transition form factors. The vector form factors

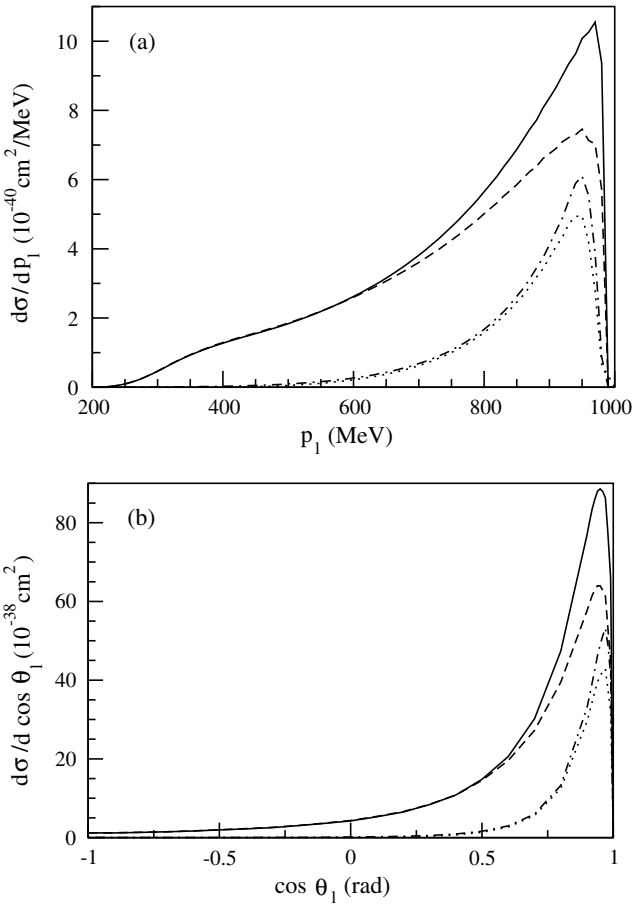

Fig. 7. The results for the differential cross-section (a) $\frac{\mathrm{d}\sigma}{\mathrm{d}p_l}$ *vs.* p_l and (b) $\frac{\mathrm{d}\sigma}{\mathrm{d}\cos\theta_l}$ *vs.* $\cos\theta_l$ at $E = 1.0\,\mathrm{GeV}$ in the present model with Pauli suppression (solid line for ν_μ and dash-dotted line for $\bar{\nu}_\mu$) and with nuclear effects (dashed line for ν_μ and dotted line for $\bar{\nu}_\mu$).

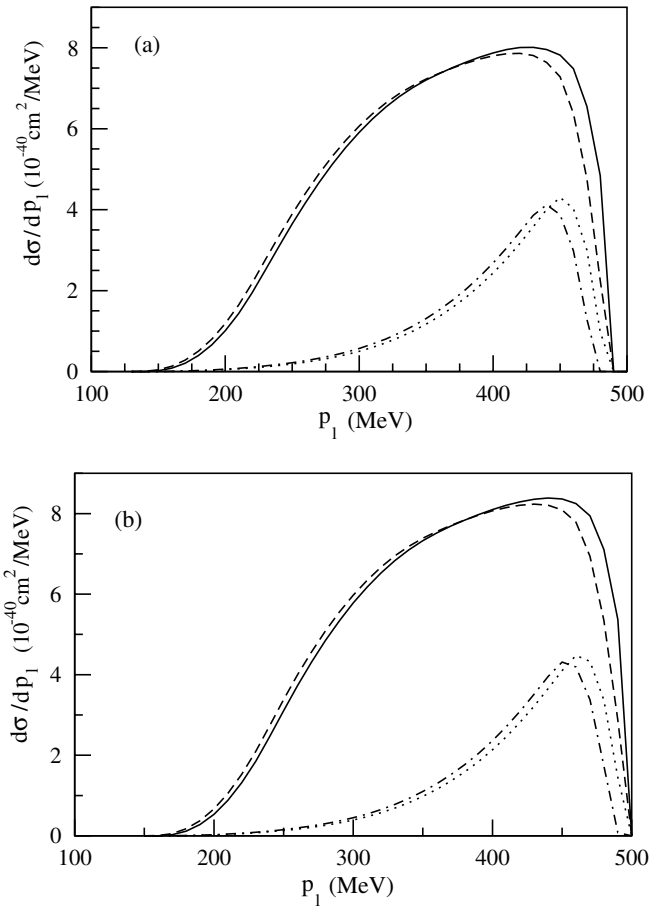

Fig. 8. Differential scattering cross-section $\frac{\mathrm{d}\sigma}{\mathrm{d}p_l}$ *vs.* p_l for $E_\nu = 500\,\mathrm{MeV}$, with Coulomb effect (solid line for ν_l and dash-dotted line for $\bar{\nu}_l$) and without Coulomb effect (dashed line for ν_l and dotted line for $\bar{\nu}_l$). (a) is for electron-type and (b) for muon-type neutrinos.

C_i^V $(i = 3$–$6)$ are determined by using the conserved vector current (CVC) hypothesis which gives $C_6^V(q^2) = 0$ and relates $C_i^V(i = 3, 4, 5)$ to the electromagnetic form factors which are determined from photoproduction and electroproduction of Δ's. Using the analysis of these experiments [52,53] we take for the vector form factors

$$C_5^V = 0, \qquad C_4^V = -\frac{M}{M_\Delta} C_3^V, \qquad \text{and}$$
$$C_3^V(q^2) = \frac{2.05}{(1 - \frac{q^2}{M_V^2})^2}, \qquad M_V^2 = 0.54\,\mathrm{GeV}^2\,. \tag{16}$$

The axial vector form factor $C_6^A(q^2)$ is related to ${C_5}^A(q^2)$ using PCAC and is given by

$$C_6^A(q^2) = {C_5}^A(q^2) \frac{M^2}{{m_\pi}^2 - q^2}\,. \tag{17}$$

The remaining axial vector form factors $C^A_{i=3,4,5}(q^2)$ are taken from the experimental analysis of the neutrino experiments producing Δ's in proton and deuteron targets [54,55]. These form factors are not uniquely determined but the following parameterizations give a satisfactory fit to the data:

$$C^A_{i=3,4,5}(q^2) = C_i^A(0) \left[1 + \frac{a_i q^2}{b_i - q^2}\right] \left(1 - \frac{q^2}{{M_A}^2}\right)^{-2} \tag{18}$$

with $C_3^A(0) = 0$, $C_4^A(0) = -0.3$, $C_5^A(0) = 1.2$, $a_4 = a_5 = -1.21$, $b_4 = b_5 = 2\,\mathrm{GeV}^2$, $M_A = 1.28\,\mathrm{GeV}$. Using the hadronic current given in eq. (15), the energy spectrum of the outgoing leptons is given by

$$\frac{\mathrm{d}^2\sigma}{\mathrm{d}E_{k'}\mathrm{d}\Omega_{k'}} = \frac{1}{8\pi^3} \frac{1}{MM'} \frac{k'}{E_\nu} \frac{\frac{\Gamma(W)}{2}}{(W - M')^2 + \frac{\Gamma^2(W)}{4.}} L_{\mu\nu} J^{\mu\nu}\,, \tag{19}$$

where $W = \sqrt{(p+q)^2}$ and M' is the mass of Δ,

$$L_{\mu\nu} = k_\mu k'_\nu + k'_\mu k_\nu - g_{\mu\nu} k \cdot k' + i\epsilon_{\mu\nu\alpha\beta} k^\alpha k'^\beta,$$
$$J^{\mu\nu} = \bar{\Sigma}\Sigma J^{\mu\dagger} J^\nu\,,$$

and is calculated with the use of spin-$\frac{3}{2}$ projection operator $P^{\mu\nu}$ defined as

$$P^{\mu\nu} = \sum_{\text{spins}} \psi^\mu \bar{\psi}^\nu$$

Table 1. Coefficients of eq. (25) for an analytical interpolation of $\mathrm{Im}\Sigma_\Delta$.

	C_Q (MeV)	C_{A2} (MeV)	C_{A3}(MeV)	α	β
a	−5.19	1.06	−13.46	0.382	−0.038
b	15.35	−6.64	46.17	−1.322	0.204
c	2.06	22.66	−20.34	1.466	0.613

and given by

$$P^{\mu\nu} = -\frac{\not{p}' + M'}{2M'}\left(g^{\mu\nu} - \frac{2}{3}\frac{p'^\mu p'^\nu}{M'^2} + \frac{1}{3}\frac{p'^\mu\gamma^\nu - p'^\nu\gamma_\mu}{M'} - \frac{1}{3}\gamma^\mu\gamma^\nu\right) \quad (20)$$

In eq. (19), the decay width Γ is taken to be an energy-dependent P-wave decay width given by

$$\Gamma(W) = \frac{1}{6\pi}\left(\frac{f_{\pi N\Delta}}{m_\pi}\right)^2 \frac{M}{W}|\mathbf{q}_{\rm cm}|^3\Theta(W - M - m_\pi)\,, \quad (21)$$

where

$$|\mathbf{q}_{\rm cm}| = \frac{\sqrt{(W^2 - m_\pi^2 - M^2)^2 - 4m_\pi^2 M^2}}{2W}$$

and M is the mass of nucleon. The step function Θ denotes the fact that the width is zero for the invariant masses below the $N\pi$ threshold. $|\mathbf{q}_{\rm cm}|$ is the pion momentum in the rest frame of the resonance. When reaction (14) takes place in the nucleus, the neutrino interacts with the nucleon moving inside the nucleus of density $\rho(r)$ with its corresponding momentum $\vec{p}$ constrained to be below its Fermi momentum. The produced Δ's have no such constraints on their momentum. These Δ's decay through various decay channels in the medium. The most prominent decay mode is $\Delta \to N\pi$ which produces pions. This decay mode in the nuclear medium is slightly inhibited due to Pauli blocking of the final-nucleon momentum modifying the decay width Γ used in eq. (21). This modification of Γ due to Pauli blocking of nucleus has been studied in detail in electromagnetic and strong interactions [56]. The modified Δ decay width, *i.e.* $\tilde{\Gamma}$, is written as [56]

$$\tilde{\Gamma} = \frac{1}{6\pi}\left(\frac{f_{\pi N\Delta}}{m_\pi}\right)^2 \frac{M|\mathbf{q}_{\rm cm}|^3}{W}F(k_{\rm F}, E_\Delta, k_\Delta)\Theta(W - M - m_\pi), \quad (22)$$

where $F(k_{\rm F}, E_\Delta, k_\Delta)$ is the Pauli correction factor given by

$$F(k_{\rm F}, E_\Delta, k_\Delta) = \frac{k_\Delta|\mathbf{q}_{\rm cm}| + E_\Delta E'_{p_{\rm cm}} - E_{\rm F}W}{2k_\Delta|\mathbf{q}'_{\rm cm}|} \quad (23)$$

where $k_{\rm F}$ is the Fermi momentum, $E_{\rm F} = \sqrt{M^2 + k_{\rm F}^2}$, k_Δ is the Δ momentum and $E_\Delta = \sqrt{W + k_\Delta^2}$.

Moreover, in the nuclear medium there are additional decay channels now open due to two-body and three-body absorption processes like $\Delta N \to NN$ and $\Delta NN \to NNN$ through which Δ's disappear in the nuclear medium without producing a pion, while a two-body Δ absorption process like $\Delta N \to \pi NN$ gives rise to some more pions. These nuclear medium effects on Δ propagation are included by using a Δ propagator in which the Δ propagator is written in terms of Δ self-energy Σ_Δ. This is done by using a modified mass and width of Δ in nuclear medium, *i.e.* $M_\Delta \to M_\Delta + \mathrm{Re}\Sigma_\Delta$ and $\tilde{\Gamma} \to \tilde{\Gamma} - \mathrm{Im}\Sigma_\Delta$. There are many calculations of Δ self-energy Σ_Δ in the nuclear medium [56–59] and we use the results of [56], where the density dependence of real and imaginary parts of Σ_Δ are parametrized in the following form:

$$\mathrm{Re}\Sigma_\Delta = 40\frac{\rho}{\rho_0}\,\mathrm{MeV} \qquad \text{and}$$

$$-\mathrm{Im}\Sigma_\Delta = C_Q\left(\frac{\rho}{\rho_0}\right)^\alpha + C_{A2}\left(\frac{\rho}{\rho_0}\right)^\beta + C_{A3}\left(\frac{\rho}{\rho_0}\right)^\gamma. \quad (24)$$

In eq. (24), the term with C_Q accounts for the $\Delta N \to \pi NN$ process, the term with C_{A2} for the two-body absorption process $\Delta N \to NN$ and the term with C_{A3}

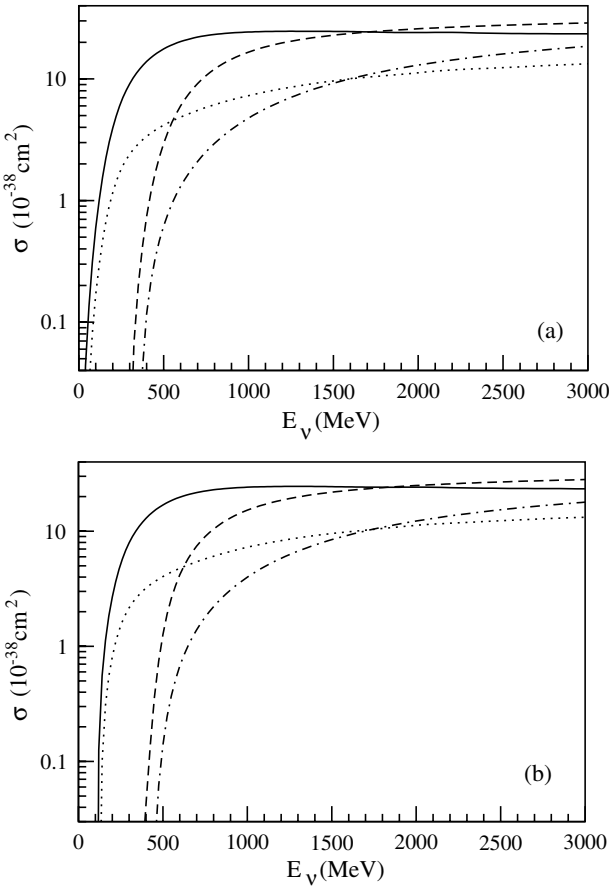

Fig. 9. The total scattering cross-section for the neutrino $\nu_l + N \to \Delta + l^-$ (shown by the dashed lines) and antineutrino $\bar{\nu}_l + N \to \Delta + l^+$ reactions (shown by dash-dotted lines) in ^{56}Fe and compared with the corresponding quasielastic cross-section in the present model with nuclear effects for the neutrino (solid lines) and antineutrino (dotted lines) reactions in ^{56}Fe. (a) is for electron-type and (b) is for muon-type neutrinos.

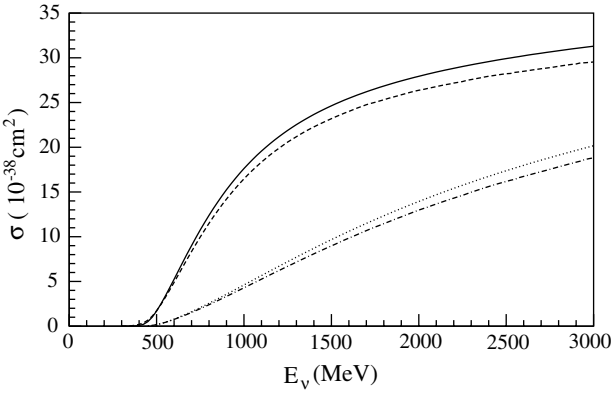

Fig. 10. Total cross-section at $E_\nu = 1.0\,\mathrm{GeV}$ for the reaction $\nu_l(\bar{\nu}_l) + N \to \Delta + l^-(l^+)$ in ^{56}Fe with (dashed line for ν_μ, dash-dotted for $\bar{\nu}_\mu$) and without nuclear effects (the solid line is the result for the ν_μ reaction and the dotted one for $\bar{\nu}_\mu$.)

for the three-body absorption process $\Delta NN \to NNN$. The coefficients C_Q, C_{A2}, C_{A3}, α, β and γ ($\gamma = 2\beta$) are parametrized in the range $80 < T_\pi < 320\,\mathrm{MeV}$ (where T_π is the pion kinetic energy) as [56]

$$C_i(T_\pi) = ax^2 + bx + c, \quad \text{for } x = \frac{T_\pi}{m_\pi}\,. \tag{25}$$

The values of the coefficients a, b and c are given in table 1. taken from ref. [56].

With these modifications, which incorporate the various nuclear medium effects on Δ propagation, the cross-section is now written as

$$\sigma = \int\int \frac{\mathrm{d}\mathbf{r}}{8\pi^3}\frac{\mathrm{d}\mathbf{k}'}{E_\nu E_l}\frac{1}{MM'} \times \frac{\frac{\tilde{\Gamma}}{2} - \mathrm{Im}\Sigma_\Delta}{(W - M' - \mathrm{Re}\Sigma_\Delta)^2 + (\frac{\tilde{\Gamma}}{2} - \mathrm{Im}\Sigma_\Delta)^2} \times \left[\rho_p(\mathbf{r}) + \frac{1}{3}\rho_n(\mathbf{r})\right] L_{\mu\nu}J^{\mu\nu}\,. \tag{26}$$

The factor $\frac{1}{3}$ in front of ρ_n comes due to suppression of charged pion production from neutron targets, *i.e.* $\nu_l + n \to l^- + \Delta^+ \to l^- + n + \pi^+$, as compared to the charged pion production from the proton target, *i.e.* $\nu_l + p \to l^- + \Delta^{++} \to l^- + p + \pi^+$, in the nucleus. In case of antineutrino reactions, $\rho_p + \frac{1}{3}\rho_n$ is replaced by $\rho_n + \frac{1}{3}\rho_p$.

3.2 Results

In this section we present results of inelastic lepton production cross-section due to Δh excitations in iron induced by the charged current neutrino interactions using eq. (26). In fig. 9(a) and (b), we show the results $\sigma(E_\nu) \sim E_\nu$ for $\nu_e(\bar{\nu}_e)$ and $\nu_\mu(\bar{\nu}_\mu)$ for the inelastic production of lepton accompanied by Δ and compare this with the cross-section for the quasielastic production of leptons discussed in sect. 2. We see that for $E_\nu \approx 1.4\,\mathrm{GeV}$ the lepton production cross-section through quasielastic and inelastic production processes are comparable. For energies $E_\nu \leq 1.4\,\mathrm{GeV}$ where the atmospheric-neutrino energies are important for fully contained events, the major contribution comes from the quasielastic events.

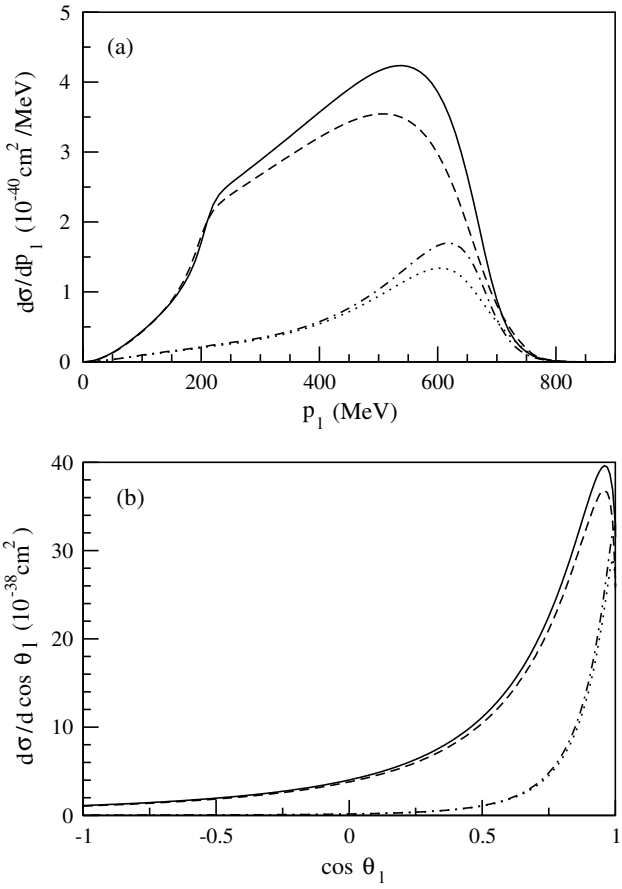

Fig. 11. Differential scattering cross-section (a) $\frac{\mathrm{d}\sigma}{\mathrm{d}p_l}$ *vs.* p_l and (b) $\frac{\mathrm{d}\sigma}{\mathrm{d}\cos\theta_l}$ *vs.* $\cos\theta_l$ at $E_\nu = 1.0\,\mathrm{GeV}$ for the reaction $\nu_l(\bar{\nu}_l) + N \to \Delta + l^-(l^+)$ in ^{56}Fe with (dashed line for ν_μ, dotted one for the $\bar{\nu}_\mu$) and without nuclear effects (the solid line is the result for the ν_μ reaction and the dash-dotted one for $\bar{\nu}_\mu$).

The effects of nuclear effects on the Δ production are shown in fig. 10 for ν_μ and $\bar{\nu}_\mu$ reactions. The results for the ν_e and $\bar{\nu}_e$ are similar to fig. 10 and are not shown here. We see that the nuclear medium effects reduce the Δ production cross-section by 5–10%.

In fig. 11(a) and (b), we show the momentum distribution $\mathrm{d}\sigma/\mathrm{d}p$ and angular distribution $\mathrm{d}\sigma/\mathrm{d}\cos\theta$ for muon-type neutrinos, where we also show the effects of nuclear effects. The nuclear medium effects reduce the cross-sections mainly in the peak region of the momentum and angular distributions for muons. The results for the momentum distribution and angular distribution for electrons is similar to the muon distributions. We show our final results on momentum and angular distributions for all charged leptons, *i.e.* e^-, e^+, μ^- and μ^+ produced in neutrino and antineutrino reactions with ν_e, ν_μ, $\bar{\nu}_e$ and $\bar{\nu}_\mu$ for $E_\nu = 1\,\mathrm{GeV}$ in fig. 12(a) and (b) in ^{56}Fe nuclei.

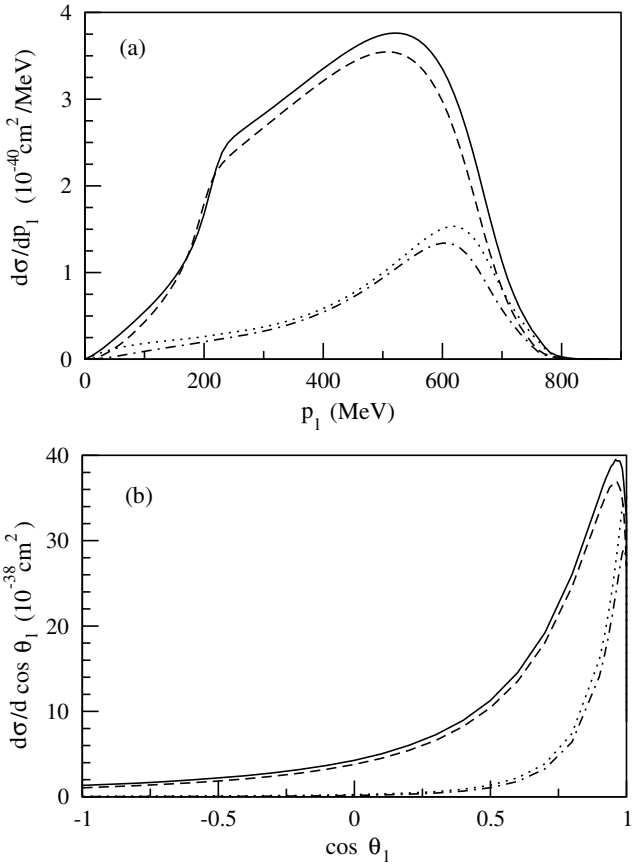

Fig. 12. The results for the differential cross-section (a) $\frac{\mathrm{d}\sigma}{\mathrm{d}p_l}$ *vs.* p_l and (b) $\frac{\mathrm{d}\sigma}{\mathrm{d}\cos\theta_l}$ *vs.* $\cos\theta_l$ with nuclear effects at $E = 1.0\,\mathrm{GeV}$ for the reaction $\nu_l(\bar{\nu}_l) + N \to \Delta + l^-(l^+)$ in ^{56}Fe. The solid line is the result for ν_e, the dashed one for ν_μ, the dotted one for $\bar{\nu}_e$ and the dash-dotted one for $\bar{\nu}_\mu$ reactions.

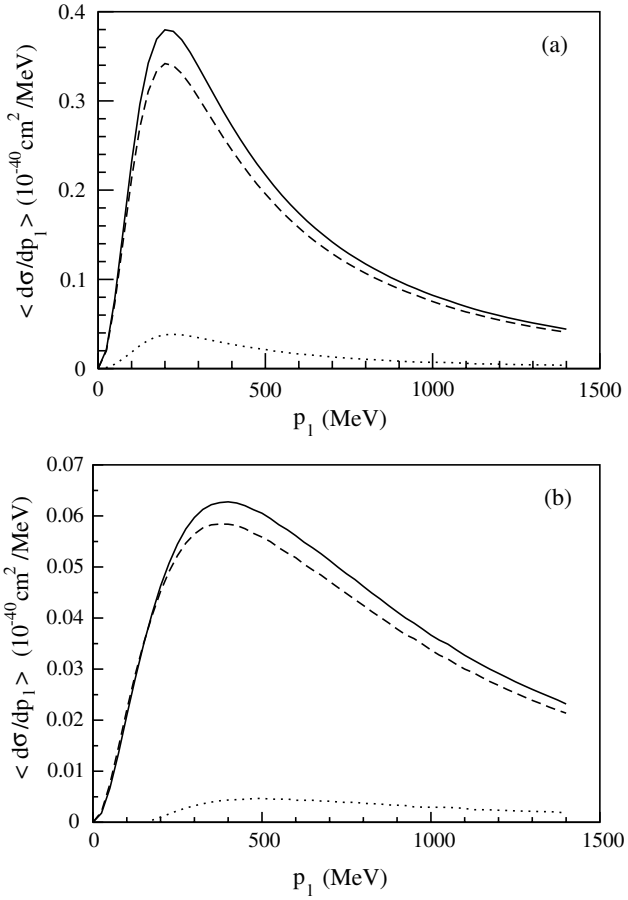

Fig. 13. Flux-averaged differential cross-section $\langle \frac{\mathrm{d}\sigma}{\mathrm{d}p_l} \rangle$ *vs.* p_l at the Soudan site simulated by Barr *et al.* [15]. (a) for $\nu_\mu + N \to \Delta + \mu^-$ and (b) for $\bar{\nu}_\mu + N \to \Delta + \mu^+$ reactions in ^{56}Fe. The solid line is for total Δ events, the dashed line is for one π production events and the dotted line is for quasielastic-like events (due to Δ absorption in the nuclear medium).

Here, we would like to make some comments about the lepton events produced through the Δ excitation. The Δ excitation process gives rise to leptons accompanied by one-pion events produced by $\Delta \to N\pi$ and $\Delta N \to \pi NN$ processes in the nuclear medium. The pions produced through these processes will undergo secondary nuclear interactions like multiple scattering and possible absorption in iron nuclei while passing through the nucleus and an appropriate model has to be used for their description. Models developed by Salcedo *et al.* [40] and Paschos *et al.* [52] have studied these effects but we do not consider these effects here as they are beyond the scope of this paper. The Δ excitation process in the nuclear medium also gives rise to quasielastic-like events through two-body and three-body absorption processes like $\Delta N \to NN$ and $\Delta N \to \Delta NN$, where only leptons are present in the final states. The quasielastic-like lepton events have been discussed by Kim *et al.* [21] but no quantitative estimates have been made. We have discussed in an earlier paper [51] this process only qualitatively but make a quantitative estimate of these events in this paper. We find that around $E_\nu = 1\,\mathrm{GeV}$ the contribution of these quasielastic-like events is about 10–12% but its effect on the flux-averaged production of leptons for atmospheric neutrinos is not very significant. This is discussed in some detail in the next section.

4 Lepton production by atmospheric neutrinos

The energy dependences of the quasielastic and inelastic lepton production cross-sections described in sects. 2 and 3 have been used to calculate the lepton production by atmospheric neutrinos after averaging over the neutrino flux corresponding to the two sites of Soudan and Gran Sasso, where iron-based detectors are being used. There are quite a few calculations of atmospheric-neutrino fluxes at these two sites. We use the angle-averaged fluxes calculated by Honda *et al.* [14] and Barr *et al.* [15] for the Soudan site and the fluxes of Barr *et al.* [15] and Plyaskin [16] for the Gran Sasso site to calculate the flux-averaged cross-section $\langle\sigma\rangle$ and also the momentum and the angular distributions $\langle \frac{\mathrm{d}\sigma}{\mathrm{d}p_l} \rangle$ and $\langle \frac{\mathrm{d}\sigma}{\mathrm{d}\cos\theta_l} \rangle$ for leptons produced by ν_e, $\bar{\nu}_e$, ν_μ and $\bar{\nu}_\mu$.

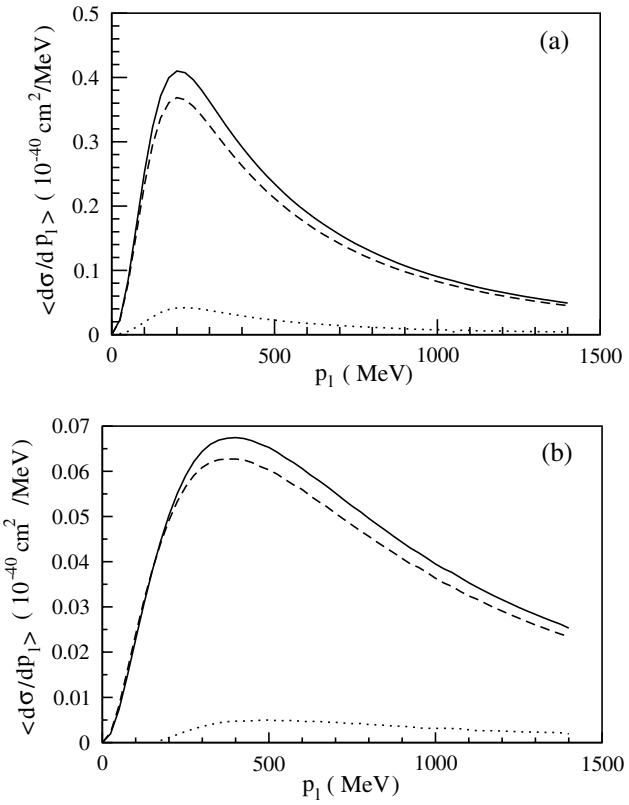

Fig. 14. Flux-averaged differential cross-section $\langle \frac{d\sigma}{dp_l} \rangle$ *vs.* p_l at the Gran Sasso site simulated by Barr *et al.* [15]. (a) for $\nu_\mu + N \to \Delta + \mu^-$ and (b) for $\bar{\nu}_\mu + N \to \Delta + \mu^+$ reactions in ^{56}Fe. The solid line is for total Δ events, the dashed line is for one-π production events and the dotted line is for quasielastic-like events (due to Δ absorption in the nuclear medium.)

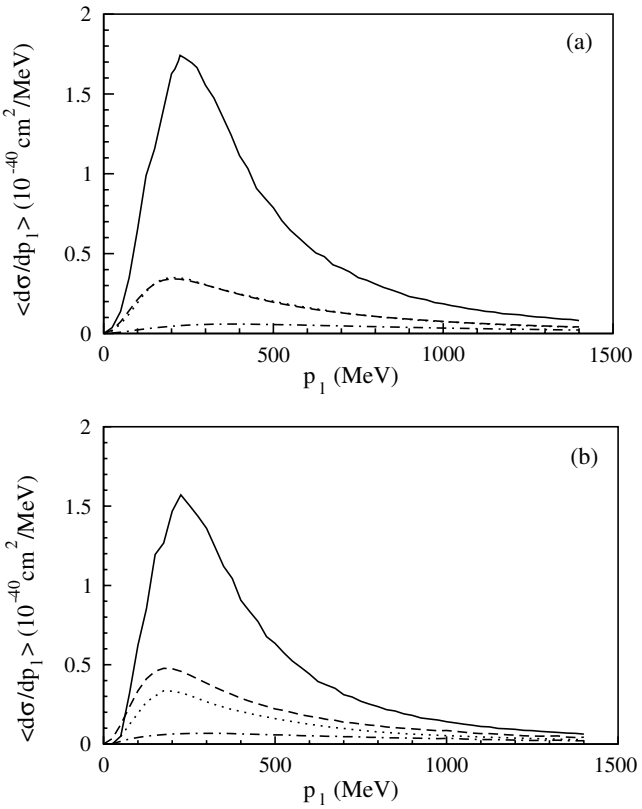

Fig. 15. Flux-averaged differential cross-section $\langle \frac{d\sigma}{dp_l} \rangle$ *vs.* p_l at the Soudan site simulated by Barr *et al.* [15]. The solid line is for total quasielastic events and the dashed line is for the one-π production events for the ν_μ reaction in ^{56}Fe. The corresponding results for $\bar{\nu}_\mu$ are shown by dotted and dash-dotted lines, (a) for muon-type and (b) for electron-type neutrinos.

4.1 Flux-averaged momentum and angular distributions

In this section we present the numerical results for the flux-averaged momentum distributions $\langle \frac{d\sigma}{dp_l} \rangle$ and angular distributions $\langle \frac{d\sigma}{d\cos\theta_l} \rangle$ for various leptons produced from ν_e, $\bar{\nu}_e$, ν_μ, $\bar{\nu}_\mu$ at the atmospheric-neutrino sites of Soudan and Gran Sasso. These leptons are produced through the quasielastic as well as inelastic processes. The quasielastic production has been discussed in sect. 2 and the inelastic production has been discussed in sect. 3. The inelastic production of leptons is accompanied by pions. However, in the nuclear medium where the production of Δ is followed by $\Delta N \to NN$, $\Delta NN \to NNN$ absorption processes, the leptons are produced without pions. These are quasielastic-like events. We show the momentum distribution of the leptons produced in iron nuclei corresponding to one-pion and quasielastic-like events for atmospheric neutrinos relevant to Soudan and Gran Sasso sites. We show it for ν_μ and $\bar{\nu}_\mu$ for the Soudan site in fig. 13(a) and (b) and for the Gran Sasso site in fig. 14(a) and (b) corresponding to the flux of Barr *et al.* [15]. We see that at both sites, the production cross-section of quasielastic-like events is quite small.

We now present our final results for the momentum distribution and angular distribution for various leptons produced by atmospheric neutrinos at Soudan and Gran Sasso sites in figs. 15-18. In these figures separate contributions from the quasielastic and inelastic processes to the momentum and angular distributions of charged leptons are shown explicitly. The quasielastic events are those where only a charge lepton is produced in the final state either by the quasielastic process described in sect. 2 or by the inelastic process of Δ production followed by its subsequent absorption in the nuclear medium as described in sect. 3. The inelastic events are those events in which a charged lepton in the final state is accompanied by a charged pion as a decay product of deltas excited in the nuclear medium.

We show the results for the momentum distribution $\langle d\sigma/dp_l \rangle \sim p_l\,(l = e^-, e^+, \mu^+, \mu^-)$ for the atmospheric-neutrino fluxes of Barr *et al.* [15] at the Soudan site in fig. 15 and at Gran Sasso site in fig. 16. We see that in all cases the major contributions to the charged lepton production comes from the quasielastic processes induced by neutrinos (solid line). The contribution from the quasielastic processes induced by antineutrinos (dotted line) and inelastic processes induced by

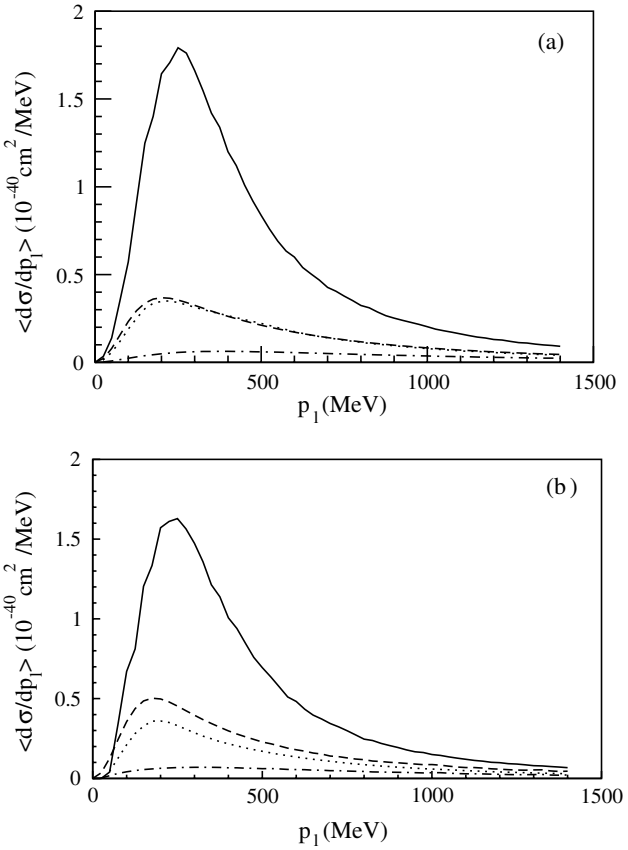

Fig. 16. Flux-averaged differential cross-section $\langle \frac{d\sigma}{dp_l} \rangle$ *vs.* p_l at the Gran Sasso site simulated by Barr *et al.* [15]. The solid line is for total quasielastic events and the dashed line is for the one-π production events for the ν_μ reaction in ^{56}Fe. The corresponding results for $\bar{\nu}_\mu$ are shown by dotted and dash-dotted lines, (a) for muon-type and (b) for electron-type neutrinos.

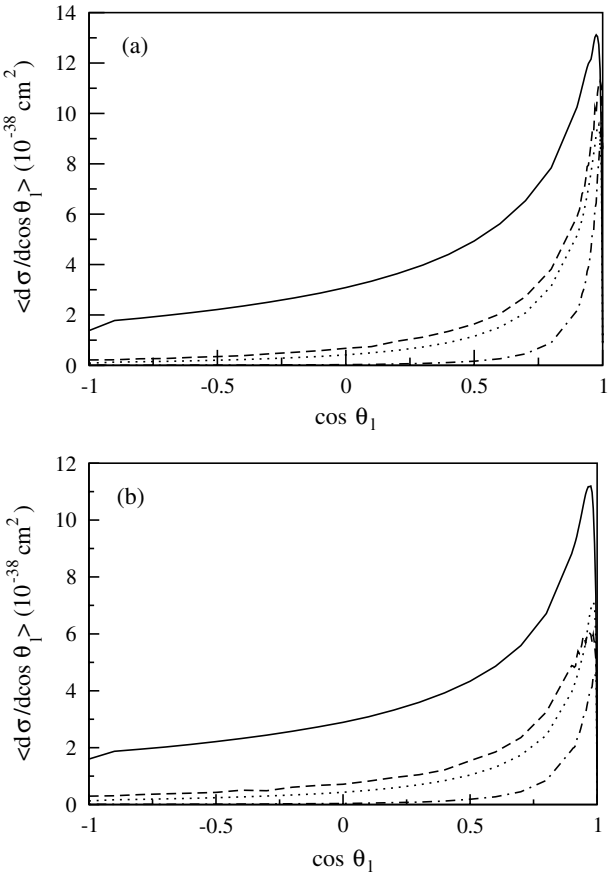

Fig. 17. Flux-averaged differential cross-section $\langle \frac{d\sigma}{d\cos\theta_l} \rangle$ *vs.* $\cos\theta_l$ at the Soudan site simulated by Barr *et al.* [15]. The solid line is for total quasielastic events and the dashed line is for the one-π production events for the ν_μ reaction in ^{56}Fe. The corresponding results for $\bar{\nu}_\mu$ are shown by dotted and dash-dotted lines, (a) for muon-type and (b) for electron-type neutrinos.

neutrinos (dashed line) is small and is around 20% in the peak region. The contribution due to inelastic processes induced by antineutrinos is very small over the whole region (dash-dotted lines).

The peak in quasielastic ν_μ reactions occurs around $p_l \approx 200\,\text{MeV}$. The peaks in the inelastic ν_μ and quasielastic $\bar{\nu_\mu}$ reactions are slightly shifted towards lower energies. The momentum distribution of the leptons for the quasielastic reaction is peaked more sharply than the momentum distribution of the inelastic reaction.

We have also presented the numerical results for angular distributions of leptons $\langle \frac{d\sigma}{d\cos\theta_l} \rangle$ *vs.* $\cos\theta$ for the atmospheric-neutrino fluxes of Barr *et al.* [15] for the Soudan site in fig. 17 and for the Gran Sasso site in fig. 18. The inelastic lepton production accompanied by pions (dashed line for $\mu^-(e^-)$ production and dash-dotted line for $\mu^+(e^+)$ production) and the quasielastic lepton production events (solid line for $\mu^-(e^-)$ production and dotted line for $\mu^+(e^+)$ production) have been explicitly shown in these figures. We see from these figures that the lepton production cross-sections are forward peaked in all cases. The inelastic distributions due to pion production are slightly more forward peaked than the quasielastic distribution. The contributions of the inelastic lepton events are small compared to the quasielastic events and the angular distributions of the flux-averaged cross-sections are dominated by the quasielastic events.

At the Soudan site, we have also studied the momentum and angular distributions for the atmospheric-neutrino fluxes of Honda *et al.* [14]. We find that the momentum and angular distributions for the production of muons are similar to the distributions obtained for the flux of Barr *et al.* [15]. In the case of electron production, the use of the flux of Honda *et al.* [14], gives a slightly smaller value for $\langle d\sigma/dp_l \rangle$ and $\langle \frac{d\sigma}{d\cos\theta_l} \rangle$ for electrons as compared to the flux of Barr *et al.* [15].

Similarly, at the Gran Sasso site, the momentum and angular distributions for the atmospheric-neutrino fluxes of Plyaskin [16] have also been studied. Here, we also find that the momentum and angular distributions for the production of muons are similar to the distributions obtained for the flux of Barr *et al.* [15]. In the case of electron production, the use of the flux of Plyaskin [16] gives a slightly

Table 2. Ratio $R = R_{\mu/e} = \frac{Y_\mu + Y_{\bar{\mu}}}{Y_e + Y_{\bar{e}}}$ corresponding to quasielastic, inelastic and total production of leptons (FG refers to the Fermi gas model, NM refers to the nuclear model, FN refers to the free nucleon, ΔN refers to Δ in the nuclear model, ΔF refers to Δ free). R_F shows the ratio of total lepton yields for muon to electron for the case of the free nucleon and R_N shows the ratio of total yields for muon to electron for the case of nucleon in the nuclear medium.

Site	Soudan	Soudan	Soudan	Gran Sasso	Gran Sasso
FLUX	Barr *et al.* [15]	Plyaskin [16]	Honda *et al.* [14]	Barr *et al.* [15]	Plyaskin [16]
Quasielastic					
R_{NM}	1.80	1.65	1.89	1.95	2.00
R_{FG}	1.81	1.66	1.89	1.95	2.09
R_{FN}	1.82	1.68	1.90	1.95	2.08
Inelastic					
$R_{\Delta N}$	1.84	1.81	1.95	2.02	2.05
$R_{\Delta F}$	1.82	1.80	1.94	2.01	2.03
Total					
R_N	1.81	1.68	1.90	1.96	2.01
R_F	1.82	1.69	1.90	1.96	2.07

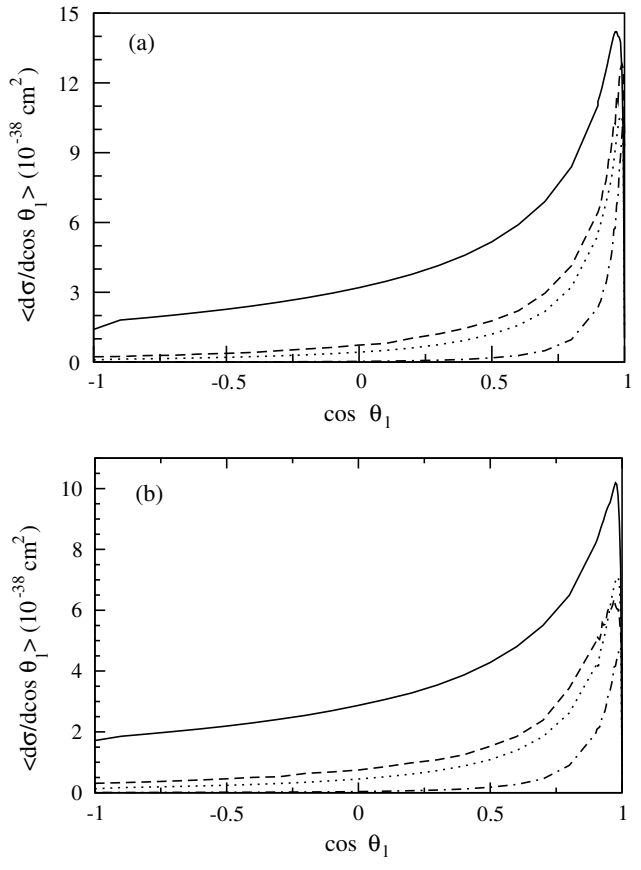

Fig. 18. Flux-averaged differential cross-section $\langle \frac{\mathrm{d}\sigma}{\mathrm{d}\cos\theta_l} \rangle$ *vs.* $\cos\theta_l$ at the Gran Sasso site simulated by Barr *et al.* [15]. The solid line is for total quasielastic events and the dashed line is for the one-π production events for the ν_μ reaction in ^{56}Fe. The corresponding results for $\bar{\nu}_\mu$ are shown by dotted and dash-dotted lines, (a) for muon-type and (b) for electron-type neutrinos.

smaller value for $\langle \mathrm{d}\sigma/\mathrm{d}p_l \rangle$ and $\langle \frac{\mathrm{d}\sigma}{\mathrm{d}\cos\theta_l} \rangle$ for electrons as compared to the flux of Barr *et al.* [15].

We further find that for the flux of Barr *et al.* [15], the lepton production cross-section at the Soudan site is slightly larger than at the Gran Sasso site for muons as well as for electrons.

4.2 Flux-averaged total cross-sections and lepton yields

The total cross-sections for the production of leptons and its energy dependence have been discussed in sect. 2 and sect. 3 for quasielastic and inelastic reactions. In this section we calculate the lepton yields Y_l for lepton of flavor l which we define as

$$Y_l = \int \Phi_{\nu_l}\ \sigma(E_{\nu_l})\ \mathrm{d}E_{\nu_l}\,,$$

where Φ_{ν_l} is the atmospheric-neutrino flux of ν_l and $\sigma(E_{\nu_l})$ is the total cross-section for neutrino ν_l of energy E_{ν_l}. We calculate this yield separately for the quasielastic and inelastic events. We define a relative yield of muon- over electron-type events by R as $R = R_{\mu/e} = \frac{Y_\mu + Y_{\bar{\mu}}}{Y_e + Y_{\bar{e}}}$ for quasielastic and inelastic events and present our results in table 2. We study the nuclear model dependence as well as the flux dependence of the relative yield R.

The results for R are presented separately for quasielastic events, inelastic events and the total events in table 2. For quasielastic events $\nu_l(\bar{\nu}_l) + {}^{56}\mathrm{Fe} \to l^-(l^+) + X$, the results are presented for the case of the free nucleon by R_{FN}, for the nuclear case with the Fermi gas model description of Llewellyn Smith [20] by R_{FG} and for the case of nuclear effects within our model by R_{NM}. We see that there is practically no nuclear-model dependence on the value of R (compare the values of R_{NM},

Table 3. % ratio $r = \frac{Y_\Delta}{Y_{\text{q.e.}+\Delta}}$ (N refers to the nuclear model, F refers to free case).

Sites	Soudan	Soudan	Soudan	Gran Sasso	Gran Sasso
FLUX	Barr *et al.* [15]	Plyaskin [16]	Honda *et al.* [14]	Barr *et al.* [15]	Plyaskin [16]
$r_\mu(F)$	14	12	14	15	12
$r_e(F)$	14	11	14	14	12
$r_\mu(N)$	22	20	22	23	19
$r_e(N)$	22	19	22	22	19

R_{FG} and R_{FN} for the same fluxes at each site). This is also true for the inelastic production of leptons, *i.e.* $\nu_l(\bar{\nu}_l) + {}^{56}\text{Fe} \to l^-(l^+) + \pi^+(\pi^-) + X$ for which the ratio for the free-nucleon case (denoted by $R_{\Delta F}$) and the ratio for the nuclear case in our model (denoted by $R_{\Delta N}$) are presented in table 2. It is, therefore, concluded that there is no appreciable nuclear-model dependence on the ratio of total lepton yields for the production of muons and electrons (compare the values of R_F and R_N, where R_F shows the ratio of total lepton yields for muon and electron for the case of the free nucleon and R_N shows the ratio of total yield for muon and electron for the case of the nucleon in the nuclear medium).

However, there is some dependence of the ratio R on the atmospheric-neutrino fluxes. The flux dependence of R can be readily seen from table 2, for the two sites of Soudan and Gran Sasso. At the Gran Sasso site, we see that there is 4–5% difference in the value of R_N for the total lepton yields for the fluxes of Barr *et al.* [15] and Plyaskin [16]. At the Soudan site, the results for the fluxes of Honda *et al.* [14] and Barr *et al.* [15] are within 4–5% but the flux calculation of Plyaskin [16] gives a result which is about 10–11% smaller than the results of Honda *et al.* [14] and 7–8% smaller than the results of Barr *et al.* [15]. The flux dependence is mainly due to the quasielastic events. This should be kept in mind while using the flux of Plyaskin [16] for making any analysis of the neutrino oscillation experiments.

In table 3, we present a quantitative estimate of the relative yield of inelastic events r_l defined by $r_l = \frac{Y_l{}^\Delta}{Y_l}$, where $Y_l{}^\Delta = Y_l{}^\Delta + Y_{\bar{l}}{}^\Delta$ is the lepton yield due to the inelastic events and Y_l is the total lepton yield due to the quasielastic and inelastic events, *i.e.* $Y_l = Y_l{}^{\text{q.e.}} + Y_{\bar{l}}{}^{\text{q.e.}} + Y_l{}^\Delta + Y_{\bar{l}}{}^\Delta$. The relative yield for the case of the free nucleon is shown by $r_l(F)$ and for the case with the nuclear effects in our model is shown by $r_l(N)$. We see that for free nucleons, the relative yield of the inelastic events due to Δ excitation is in the range 12–15% for various fluxes at the two sites. The ratio is approximately the same for electrons and muons. When the nuclear effects are taken into account this becomes 19–22%. This is due to the different nature of the effect of nuclear structure on the quasielastic and inelastic production cross-sections which gives a larger reduction in the cross-section for the quasielastic case as compared to the inelastic case. This quantitative estimate of $r_l(N)$ in iron may be compared with the results in oxygen, where the experimental results at Kamiokande give a value of 18% [60].

5 Conclusions

We have studied the charged lepton production in iron induced by atmospheric neutrinos at the experimental sites of Soudan and Gran Sasso. The energy dependence of the total cross-sections for the quasielastic and inelastic processes have been calculated in a nuclear model which takes into account the effect of the Pauli principle, Fermi motion effects and the renormalization of weak transition strengths in the nuclear medium. The inelastic process has been studied through the Δ-dominance model which incorporates the modification of mass and width of the Δ-resonance in the nuclear medium. The numerical results for the momentum and angular distributions of the charged lepton production cross-section have been presented for muons and electrons. The relative yield of muon to electron production has been studied. In addition to the nuclear-model dependence, the flux dependence of the total yields, momentum distribution $\frac{\mathrm{d}\sigma}{\mathrm{d}p_l}$ and $\frac{\mathrm{d}\sigma}{\mathrm{d}\cos\theta_l}$ have been also studied. In the following we conclude this paper by summarizing our main results:

1. There is a large reduction due to nuclear effects in the total cross-section for quasielastic production cross-section specially at lower energies (40–50% around 200 MeV) and the reduction becomes smaller at higher energies (15–20% around 500 MeV).

2. For quasielastic reactions we find a larger reduction in the total cross-section as compared to the Fermi gas model. The energy dependence of this reduction in cross-section at low energies ($E < 500\,\text{MeV}$) is found to be different for neutrino and antineutrino reactions.

3. The inelastic production of leptons where a charged lepton is accompanied by a pion, becomes comparable to the quasielastic production of leptons for $E_\nu \sim 1.4\,\text{GeV}$ and increases with the increase of energy. The effect of the nuclear medium on the inelastic production cross-section (in absence of pion re-scattering effects) in not too large ($\sim 10\%$).

4. For quasielastic reactions the effect of the Coulomb distortion of the final lepton in the total cross-section is small except at very low energies ($E < 500\,\text{MeV}$) and becomes negligible when averaged over the flux of atmospheric neutrinos.

5. The flux-averaged momentum distribution of leptons produced by atmospheric neutrinos is peaked around the momentum $p_l \sim 200\,\text{MeV}$ for electrons and muons. The peak for the quasielastic production is sharper than for the inelastic production. The inelastic production of

leptons contributes about 20% to the total production of leptons.

6. The flux-averaged angular distribution of leptons for atmospheric neutrinos for quasielastic as well as for inelastic production is sharply peaked in the forward direction.

7. There is a very little flux dependence on the relative yield of muons and electrons at the site of Gran Sasso. However, at the Soudan site, the atmospheric flux as determined by Plyaskin [16] gives a value of the relative yield which is smaller than the relative yield obtained using the flux of Honda *et al.* [14] and Barr *et al.* [15].

8. The nuclear-model dependence of the relative yield of muons to electrons is negligible, even though the individual yields for muons and electrons are reduced with the inclusion of nuclear effects specially for the quasielastic production.

The work is financially supported by the Department of Science and Technology, Government of India under the grant DST Project No. SP/S2K-07/2000. One of the authors (S. Ahmad) would like to thank CSIR for financial support.

References

1. C.V. Achar *et al.*, Phys. Lett. B **18**, 196 (1965); **19**, 78 (1965); F. Reines *et al.*, Phys. Rev. Lett. **15**, 429 (1965).
2. M.F. Crouch *et al.*, Phys. Rev. D **18**, 2239 (1978); M.R. Krishnaswamy *et al.*, Proc. R. Soc. London, Ser. A **323**, 489 (1971).
3. T.J. Haines *et al.*, Phys. Rev. Lett. **57**, 1986 (1986); D. Casper *et al.*, Phys. Rev. Lett. **66**, 2561 (1991); R. Becker-Szendy *et al.*, Phys. Rev. D **46**, 3720 (1992).
4. K.S. Hirata *et al.*, Phys. Lett. B **205**, 416 (1988); **280**, 146 (1992); Y. Fukuda *et al.*, Phys. Lett. B **335**, 237 (1994); **433**, 9 (1998); E.W. Beir *et al.*, Phys. Lett. B **283**, 446 (1992).
5. W.W.M. Allison *et al.*, Phys. Lett. B **391**, 491 (1997); **427**, 217 (1998).
6. S.M. Bilenky, C. Giunti, W. Grimus, Prog. Part. Nucl. Phys. **43**, 1 (1999); P. Langacker, J.P. Leveille, J. Scheiman, Phys. Rev. D **27**, 1228 (1983); T.K. Kuo, J. Pantaleone, Rev. Mod. Phys. **61**, 937 (1989).
7. S.N. Ahmad *et al.*, Phys. Rev. Lett. **92**, 181301 (2004); Q.R. Ahmad *et al.*, Phys. Rev. Lett. **87**, 071301 (2001).
8. K. Eguchi *et al.*, Phys. Rev. Lett. **90**, 021802 (2003).
9. T. Kajita, Y. Totsuka, Rev. Mod. Phys. **73**, 85 (2001); K. Kaneyuki, Nucl. Phys. B (Proc. Suppl.) **112**, 24 (2002); S. Fukuda *et al.*, Phys. Rev. Lett. **86** 5651; 5656 (2001).
10. G. Giacomelli, A. Margiotta, Eur. Phys. J. C **33**, S826 (2004); M. Ambrosio *et al.*, Phys. Lett. B **566**, 35 (2003); **517**, 59 (2001).
11. M. Sanchez *et al.*, Phys. Rev. D **68**, 113004 (2003); W.A. Mann, Nucl. Phys. B (Proc. Suppl.) **91**, 134 (2000); T. Kafka, Nucl. Phys. B (Proc. Suppl.) **87**, 186 (2000); W.W.M. Allison *et al.*, Phys. Lett. B **449**, 137 (1999).
12. S. Palomares-Ruiz, S.T. Petcov, Nucl. Phys. B **712**, 392 (2005); G. Altarelli, F. Feruglio, New J. Phys. **6**, 106 (2004); W.M. Alberico, S.M. Bilenky, Phys. Part. Nucl. **35**, 297 (2004).
13. M. Honda, T. Kajita, K. Kasahara, S. Midorikawa, Phys. Rev. D **70**, 043008 (2004); G. Battistoni, A. Ferrari, T. Montaruli, P.R. Sala, Astropart. Phys. **19**, 269 (2003); T.K. Gaisser, M. Honda, Annu. Rev. Nucl. Part. Sci. **52**, 153 (2002).
14. M. Honda, T. Kajita, K. Kasahara, S. Midorikawa, Phys. Rev. D **52**, 4985 (1995).
15. G. Barr, T.K. Gaisser, T. Stanev, Phys. Rev. D **39**, 3532 (1989).
16. V. Plyaskin, hep-ph/0303146 (2003).
17. T.W. Donnelly, J.D. Walecka, Phys. Lett. B **41**, 275 (1972); T.W. Donnelly, Phys. Lett. B **43**, 93 (1973); J.B. Longworthy, B.A. Lamers, H. Uberall, Nucl. Phys. A **280**, 351 (1977); E.V. Bugaev, G.S. Bisnovatyi-Kogan, M.A. Rudzsky, Z.F. Seidov, Nucl. Phys. A **324**, 350 (1979); C. Maieron, M.C. Martinez, J.A. Caballero, J.M. Udias, Phys. Rev. C **68**, 048501 (2003).
18. B. Goulard, H. Primakoff, Phys. Rev. **135**, B1139 (1964); J.S. Bell, C.H. Llewllynsmith, Nucl. Phys. B **28**, 317 (1971).
19. R.A. Smith, E.J. Moniz, Nucl. Phys. B **43**, 605 (1972); T.K. Gaisser, J.S. O'Connell, Phys. Rev. D **34**, 822 (1986); A.C. Hayes, I.S. Towner, Phys. Rev. C **61**, 044603 (2000); T. Kuramoto, M. Fukugita, Y. Kohyama, K. Kubodera, Nucl. Phys. A **512**, 711 (1990); A.K. Mann, Phys. Rev. D **48**, 422 (1993); G. Co, C. Bleve, I. De Mitri, D. Martello, Nucl. Phys. (Proc. Suppl.) **112**, 210 (2002), J.M. Udias, P.J. Mulders, Phys. Rev Lett. **74**, 4993 (1995); H. Nakamura, R. Seki, Nucl. Phys. (Proc. Suppl.) **112**, 197 (2002).
20. C.H. Llewellyn Smith, Phys. Rep. **3**, 261 (1972).
21. H. Kim, J. Piekarewicz, C.J. Horowitz, Phys. Rev. C **51**, 2739 (1995).
22. J. Engel, E. Kolbe, K. Langanke, P. Vogel, Phys. Rev. D **48**, 3048 (1993); N. Auerbach, N. Van Giai, O.K. Vorov, Phys. Rev. C **56**, 2368 (1997); E. Kolbe, K. Langanke, F.K. Thielmann, P. Vogel, Phys. Rev. C **52**, 3437 (1995); E. Kolbe, K. Langanke, S. Krewald, Phys. Rev. C **51**, 1122 (1995); D.A. Krakauer *et al.*, Phys. Rev. C **45**, 2450 (1992); J. Marteau, Nucl. Phys. (Proc. Suppl.) **112**, 203 (2002); Eur. Phys. J. A **5**, 183 (1999)
23. S.K. Singh, E. Oset, Phys. Rev. C **48**, 1246 (1993).
24. M. Sajjad Athar, S.K. Singh, Phys. Lett. B **591**, 69 (2004); Phys. Rev. C **61**, 028501 (2000); T.S. Kosmas, E. Oset, Phys. Rev. C **53**, 1409 (1996); S.K. Singh, M. Sajjad Athar, Nucl. Phys. B (Proc. Suppl.) **215**, 219 (2002).
25. K. Daum *et al.*, Z. Phys. C **66**, 417 (1995).
26. M. Aglietta *et al.*, Europhys. Lett. **8**, 611 (1989).
27. M.V. Diwan, Nucl. Phys. (Proc. Suppl.) **123**, 272 (2003); H. Gallagher, Nucl. Phys. B (Proc. Suppl.) **215**, 188 (2002).
28. T.T. de Fatis, hep-ph/0106252 (2001); N.Y. Ahafonova *et al.*, proposal LNGS-P26-2000.
29. G. Rajasekharan, hep-ph/0402246 (2004).
30. A. Gil,J. Nieves, E. Oset Nucl. Phys. A **627**, 543 (1997); R.C. Carrasco, E. Oset, Nucl. Phys. A **536**, 445 (1992).
31. N.C. Mukhopadhyay, H.C. Chiang, S.K. Singh, E. Oset, Phys. Lett. B **434**, 7 (1998); H.C. Chiang, E. Oset, P. Fernandez de Cordoba Nucl. Phys. A **510**, 591 (1990).
32. S.K. Singh, E. Oset, Nucl. Phys. A **542**, 587 (1992).
33. C. Athanassopoulos, Phys. Rev. C **58**, 2489 (1998); B. Armbruster *et al.*, Phys. Rev. D **65**, 112001 (2002).
34. H. Gallagher, MINOS internal report.
35. C. Berger *et al.*, Phys. Lett. B **245**, 305 (1990).

36. C. Volpe, N. Auerbach, G. Colo, N. Van Giai, Phys. Rev. C **65**, 044603 (2002); J. Engel Phys. Rev. C **57**, 2004 (1998).
37. C. Giusti, P.D. Pacati, Nucl. Phys. A **47**, 3 (1987)717; P. Gueye *et al.*, Phys. Rev. C **60**, 044308 (1999).
38. E. Oset, D. Strottman, H. Toki, J. Navarro, Phys. Rev. C **48**, 2395 (1993); E. Oset, P. Fernandez de Cordoba, L.L. Salcedo, R. Brockmann, Phys. Rep. **188**, 79 (1990).
39. C. Garcia Recio, E. Oset, L.L. Salcedo, Phys. Rev. C **37**, 194 (1988).
40. L.L. Salcedo, E. Oset, M.J. Vicente Vacas, C. Garcia Recio, Nucl. Phys. A **484**, 557 (1988); E. Oset, in *SERC School of Nuclear Physics*, edited by B.K. Jain (World Scientific, 1987).
41. H. de Vries, C.W. de Jager, C. de Vries, At. Data Nucl. Data Tables **36**, 495 (1987).
42. LSND Collaboration (L.B. Auerbach *et al.*), Phys. Rev. C **66**, 015501 (2002).
43. S. Bonnetti *et al.*, Nuovo Cimento A **38**, 260 (1977).
44. J. Brunner *et al.*, Z. Phys. C **45**, 551 (1990).
45. M. Pohl *et al.*, Lett. Nuovo Cimento **26**, 332 (1979).
46. A.A. Belikov, Z. Phys. A **320**, 625 (1985).
47. N.J. Baker *et al.*, Phys. Rev. B **23**, 2499 (1981); K.L. Miller *et al.*, Phys. Rev. D **26**, 537 (1982); T. Kitagaki *et al.*, Phys. Rev. D **28**, 4366 (1983); **34**, 2554 (1986); **42**, 1331 (1990).
48. M. Sajjad Athar, S. Ahmad, S.K. Singh, to be published in the *Proceedings of the School on Non-Accelerator Astroparticle Physics, held at ICTP, Trieste, Italy, July 2004.*
49. S.L. Adler, Ann. Phys. (N.Y.) **50**, 189 (1968); P.A. Schreiner, F. Von Hippel, Nucl. Phys. B **58**, 333 (1973); G.L. Fogli, G. Nardulli, Nucl. Phys. B **160**, 116 (1979); **165**, 162 (1980); D. Rein, L.M. Sehgal, Ann. Phys. (N.Y.) **133**, 79 (1981); E.A. Paschos, Nucl. Phys. B (Proc. Suppl.) **112**, 89 (2002); E.A. Paschos, L. Pasquali, J.Y. Yu, Nucl. Phys. B **588**, 263 (2000); E.A. Paschos, J.Y. Yu, Phys. Rev. D **65**, 033002 (2002).
50. S.L. Adler, S. Nussinov, E.A. Paschos, Phys. Rev. D **9**, 2125 (1974); H. Kim, S. Schramm, C.J. Horowitz, Phys. Rev. C **53**, 2468; 3131 (1996).
51. S.K. Singh, M.J. Vicente Vacas, E. Oset, Phys. Lett. B **416**, 23 (1998).
52. E.A. Paschos, J.Y. Yu, M. Sakuda, Phys. Rev. D **69**, 014013 (2004).
53. A.J. Dufner, Y.S. Tsai, Phys. Rev. **168**, 1801 (1968); G. Olsson *et al.*, Phys. Rev. D **17**, 2938 (1978).
54. T. Kitagaki *et al.*, Phys. Rev. D **42**, 1331 (1990); **34**, 2554 (1986).
55. S.J. Barish *et al.*, Phys. Rev. D **19**, 2521 (1979); G.M. Radecky *et al.*, Phys. Rev. D **25**, 1161 (1982).
56. E. Oset, L.L. Salcedo, Nucl. Phys. A **468**, 631 (1987); C. Garcia Recio, E. Oset, L.L. Salcedo, D. Strottman, M.J. Lopez, Nucl. Phys. A **526**, 685 (1991).
57. E. Oset, W. Weise, Phys. Lett. B **77**, 159 (1978); Nucl. Phys. A **319**, 477 (1979); E. Oset, Y. Futami, H. Toki, Nucl. Phys. A **448**, 597 (1986).
58. H.M. Hofmann, Z. Phys. A **289**, 273 (1979); M. Hirata, F. Lenz, K. Yazaki, Ann. Phys. (N.Y.) **120**, 205 (1979).
59. E. Oset,H. Toki, W. Weise, Phys. Rep. **83**, 282 (1982); E. Oset, L.L. Salcedo, D. Strottman, Phys. Lett. B **165**, 13 (1985).
60. T. Kajita, in *Physics and Astrophysics of Neutrinos*, edited by M. Fukugita, A. Suzuki (Springer-Verlag, Tokyo, 1994).